NANO LETTERS

pubs.acs.org/NanoLett

Drude Relaxation Rate in Grained Gold Nanoantennas

Kuo-Ping Chen, Vladimir P. Drachev,* Joshua D. Borneman, Alexander V. Kildishev, and Vladimir M. Shalaev

Birck Nanotechnology Center and School of Electrical and Computer Engineering, Purdue University, 1205 West State Street, West Lafayette, Indiana 47907

ABSTRACT The effect of grain boundaries on the electron relaxation rate is significant even for large area noble metal films and more so for plasmonic nanostructures. Optical spectroscopy and X-ray diffraction show a substantial improvement in plasmon resonance quality for square-particle nanoantennas after annealing due to an enlarged grain size from 22 to 40 nm and improved grain boundaries described by the electron reflection coefficient. The electron relaxation rate due to the grains is shown to decrease by a factor of 3.2.

KEYWORDS Plasmonics, nanoantennas, electron relaxation rate, grain structure, annealing

Nanoantennas formed by coupled noble metal particles enable the plasmon resonance and strong enhancement of the local electromagnetic field in the gap which can be tuned to different frequencies.[1] The localized surface plasmon resonances and highly confined electromagnetic fields produced by nanoantennas make possible many applications including nanometer-scale photolithography,[2] nonlinear optics,[3] biosensors, optical trapping, solar energy harvesting, fluorescence enhancement,[4,5] and improved near-field scanning optical microscopy. Gold and silver are appropriate plasmonic materials for the visible range due to their low electron relaxation rates, high plasma frequency, and high-frequency interband transitions.[6,7] Although silver has a lower electron relaxation rate than gold, gold is widely used, especially in biological applications or fluidic environment experiments due to biocompatibility and higher chemical stability.[8]

Overall, the parameter of greatest interest is the Drude relaxation rate Γ, which is inversely proportional to the intraband electron relaxation time τ at optical frequencies, i.e., $\Gamma = h\tau^{-1}$, where h is Planck's constant, and which is the primary parameter quantifying the nanoantenna resonance quality. Typically, decreased resonance quality due to grain boundary effect is either commented on, but not addressed, in the literature or is invoked qualitatively. For nanostructures, this effect is less studied but typically more important than for large area metal films, because of the more complicated fabrication procedure.[9] The effect of grains on the surface-plasmon polariton propagation length was studied recently,[10] but the grain size there was determined from atomic force microscopy images, which usually give a rough estimate since it does not probe an intrinsic grain structure. We have determined both the Drude relaxation rate from optical transmission and reflection measurements and the grain properties from the X-ray diffraction (XRD) measurements. To analyze the results of our experiments, we use a quantitative model based on the linearized Boltzmann equation.[11]

Many previous works have shown that annealing improves the quality of large area metal films.[6,7,12,13] However, we have found that this is not always true for metal nanostructures. Specifically, annealing does not improve the quality of high aspect ratio nanostructures, such as nanostrips with a width less than 80 nm. Moreover, heating high aspect ratio structures initiates structural Rayleigh instability, resulting in segmentation into randomly sized pieces. In this paper we present nanostructures whose resonance properties can be substantially improved through annealing. The plasmon resonance width is affected by the change in electron relaxation rate. Another potential reason could be inhomogeneous broadening due to the geometrical effect of roughness as we observed in our previous paper[14] for paired strips. This effect is less contributive due to better quality of the square shape particles. It is shown that the decrease in the electron relaxation rate correlates with an increase in the mean crystalline size, as measured by X-ray diffraction. Additionally, our analysis based on a grain boundary scattering model[11] shows that the strength of the potential barriers at the grain boundaries, expressed in terms of electron reflection coefficient, is also reduced after annealing.

During fabrication, many factors affect the resulting quality of the gold nanoantenna and therefore change the dielectric constant of gold. The resulting gold dielectric constant may be calculated using the Drude–Lorentz model in eq 1

* Corresponding author, vdrachev@purdue.edu.
Received for review: 11/6/2009
Published on Web: 02/03/2010

DOI: 10.1021/nl9037246 | *Nano Lett.* **2010,** *10,* 916–922

$$\varepsilon = 1 - \frac{{\omega_p}^2}{\omega^2 + i\alpha\Gamma_p\omega} + \sum_m \frac{f_m {\omega_m}^2}{{\omega_m}^2 - \omega^2 - i\Gamma_m\omega} \quad (1)$$

The Drude−Lorentz model has two terms: the Drude term for the free-electron resonance, and the sum of the Lorentz terms, representing interband transitions. Here ω_p is the plasmon frequency and Γ_p is the damping constant for the Drude term. α is a loss factor used to quantify the difference between the damping term in bulk from the literature[7] and our fabricated sample. Lattice defects and grain boundaries will increase the damping constant, because the total damping term (Γ_p) is the sum of the collision rate from electrons−electrons, electrons−phonons, and electron−grain boundaries. Therefore, film defects increase the gold damping constant, quantified as having a larger α. As this work will show, the internal damping may be reduced by annealing the sample after fabrication in order to enlarge the grains and reduce the number of grain boundaries. Potentially, surface roughness may also increase the relaxation rate of electrons. However, three-dimensional simulations of nanoantenna roughness, which will be discussed later, and previous simulations and experiments for two-dimensional magnetic gratings with a root-mean-square (rms) roughness of up to 6 nm,[14] show little change in the relaxation rate as a function of roughness.

Because gold square-particle nanoantennas have a strong coupled plasmonic resonance, spectra that can be well matched using numerical simulations, and a low aspect ratio, this work uses gold nanoantennas to examine the effect of different annealing temperatures. The annealing process has been widely used in the semiconductor industry and for thin-film fabrication for decades. In thin-film fabrication, the main purpose of annealing is to decrease the intrinsic and extrinsic defects caused by fabrication.[15] Many papers discuss the effect of annealing on continuous films,[15] island films,[16] and composite films.[17] Also, some work has been done on the laser heating effect on gold nanopaticles.[18,19] Previous studies[18,19] show that enough energy may result in shape changes or even the jumping and coalescing of the nanoparticles.[20] A blue-shifted resonance wavelength and a sharper resonance peak are shown in their results.[17,20] The previous studies explain this spectra modification by reason of a change in particle shape. However, we find that under low temperature annealing, not only do the dimensions have a minor change but the material property is also improved. Therefore, gold square-particle nanoantennas with different annealing temperatures of up to 400 °C are tested in this work. Far-field transmission and reflection spectra measurement will be compared to a numerical simulation model to show the relationship between plasmonic resonance and loss factor. The field-emission scanning electron microscope (FE-SEM), atomic force microscope (AFM), and XRD measurements characterize the changes in nanoantennas after annealing treatment. Additionally the reason for improvement of the plasmonic resonance will be discussed.

Our gold nanoantenna structures are fabricated on a 15 nm indium−tin−oxide (ITO)-coated glass substrate. For E-beam lithography, PMMA A2 (MicroChem Corp.) photoresist is spin-coated onto the ITO glass substrate at 3000 rpm for 60 s. Following a 1 h prebake of the photoresist at 160 °C, an E-beam direct writing system (Vistec) is used to define the pattern with 100 kV, 765 pA, and 800 uC/cm^2. Methyl isobutyl ketone (MIBK)/isopropanol (IPA) (1:3) is used to develop the photoresist for 45 s and O_2 plasma ashing (Branson) at 100 W for 5 s is used for the descum process to remove residual photoresist for improved lift-off. Then, electron beam evaporation is used to produce a 5 nm adhesion layer of titanium and a 30 nm gold film with a 0.5 Å/s deposition rate in a 7×10^{-7} Torr vacuum chamber (Airco). After film deposition, lift-off is performed by immersion in Remover PG (MicroChem Corp.) for 6 h.

Following fabrication, annealing is done using both a hot plate and a rapid thermal processing system (RTP, Minipulse RTA), for 2 min, at 12 different temperatures from room temperature (20 °C) up to 400 °C. After annealing, the far-field transmission and reflection spectra are measured for both the primary (x), E-field perpendicular to the antenna gap, and for the secondary (y) polarization, E-field parallel to the gap. FE-SEM (Hitachi S-4800) and AFM (Veeco Dimension) measurements are used in order to profile the surface structure and roughness. XRD (PANalytical X'Pert) $\theta/2\theta$ deflection measurement is used to obtain the average grain size.

Figure 1a shows the nanoantenna design. The square particle dimensions are 100 nm × 100 nm with a thickness of 30 nm. The gap between the particles is 30 nm, and the period is 400 nm in both the x and y directions. The FE-SEM image in Figure 1b shows not only the good lift-off condition of the nanoantennas but also the well-controlled particle dimensions and gap.

Figure 2 shows the far-field transmission spectra of the sample from 500 to 900 nm with different annealing temperatures and incident light with both x (Figure 2a) and y (Figure 2b) polarizations. As the annealing temperature is increased, the resonance wavelength (λ_r) shifts to shorter wavelengths and the resonance full width at half-maximum (fwhm$_r$) becomes smaller (Table 1). A plot comparing the resonance wavelength versus annealing temperature is shown in Figure 3a. For both x and y polarizations, the resonance wavelengths have an obvious blue shift between room temperature and 225 °C. For x polarization, the wavelength shift is 27 nm, and only 7 nm for y polarization. Because the surface energy of gold is higher than that of the ITO surface, and due to the nanoantennas z:x aspect ratio of 1:3, 400 °C annealing causes the particle to contract by about 3% in the $x-y$ plane. This change in dimensions is likely the reason for the resonance shift.[1] Due to the coupled dipole resonance for the x polarization, the shift for the x

DOI: 10.1021/nl9037246 | Nano Lett. 2010, 10, 916–922

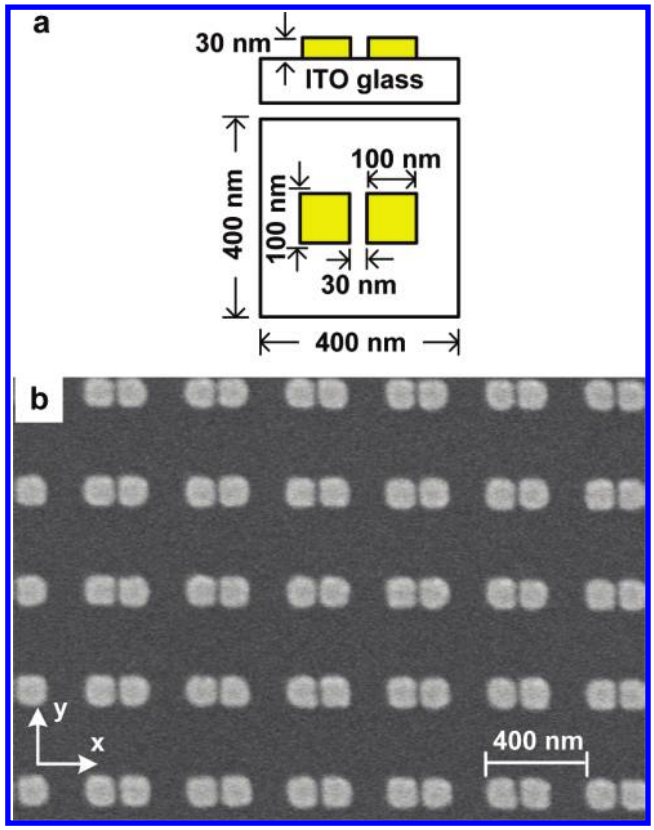

FIGURE 1. (a) Schematic of the nanoantenna unit cell (side and top view). (b) FE-SEM image of a nanoantenna array (scale bar is 400 nm).

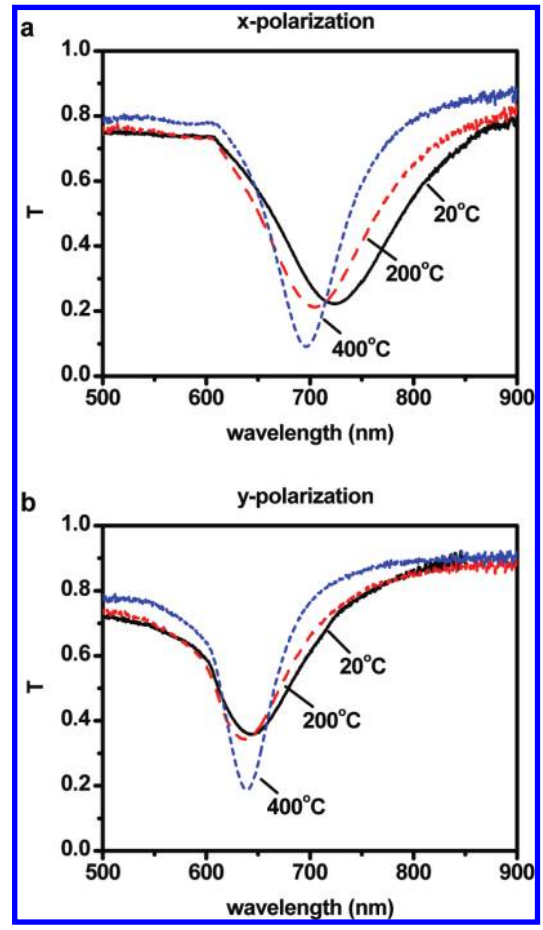

FIGURE 2. Transmission spectra from the sample after different annealing temperatures for (a) *x* polarization and (b) for *y* polarization. The black solid line is before annealing (i.e., at 20 °C); red dashed line is after annealing at 200 °C; blue short dashed line is after annealing at 400 °C.

polarization is stronger than that for the *y* polarization. A plot of the fwhm of both polarizations' resonance with respect to different annealing temperatures is shown in Figure 3b. Between 100 and 325 °C, annealing changes the resonance width for the *x* polarization; for the *y* polarization, the resonance width is modified between 200 and 325 °C.

Our observations show that there are no substantial changes in the particle shape at the annealing point, 400 °C. There is also not much difference for 500 °C, and the particles become quasi-spherical in shape after annealing at 700 °C for 2 min. This means that the swell point is between 500 and 700 °C. According to the literature[21] the grains grew by a grain boundary migration but not by coalescence of the grains in the range above the room temperature. Therefore the swell point is higher than the annealing temperatures used here since coalescence starts typically at about half of the melting temperature.

In addition to minor changes in surface quality and geometric dimensions, annealing is believed to cause significant internal grain growth. The process of grain growth has been studied for quite some time[22] and is described by grain boundary migration.[21] If the grain size is small compared with the film thickness, then the grain structure and the grain growth process are three-dimensional. As the grains grow to become equal to the film thickness, most grains traverse the entire thickness of the film, at which point

TABLE 1. Comparison of the Nanoantennas before and after Annealing

	before annealing		after annealing	
	x polarization	*y* polarization	*x* polarization	*y* polarization
λ_r, nm	725	645	698	638
$fwhm_r$, nm	115.5	83.6	77.6	55.7
loss factor	3.53		1.35	
roughness, nm	2.6		1.7	
grain size, nm	22		40	

the surface energy associated with the two free surfaces of the film becomes comparable with the surface energy of the grain boundaries. As a result, grooves may develop on the surface along lines where the grain boundaries meet the free surface. This prevents the boundaries from further migrating and leads to grain-growth stagnation. Another possible effect is that differences in the free surface energy for grains with different crystallographic orientation may provide a driving force for the migration of the boundaries that is additional to that provided by grain boundary capillarity. Grains with

DOI: 10.1021/nl9037246 | *Nano Lett.* **2010,** *10,* 916–922

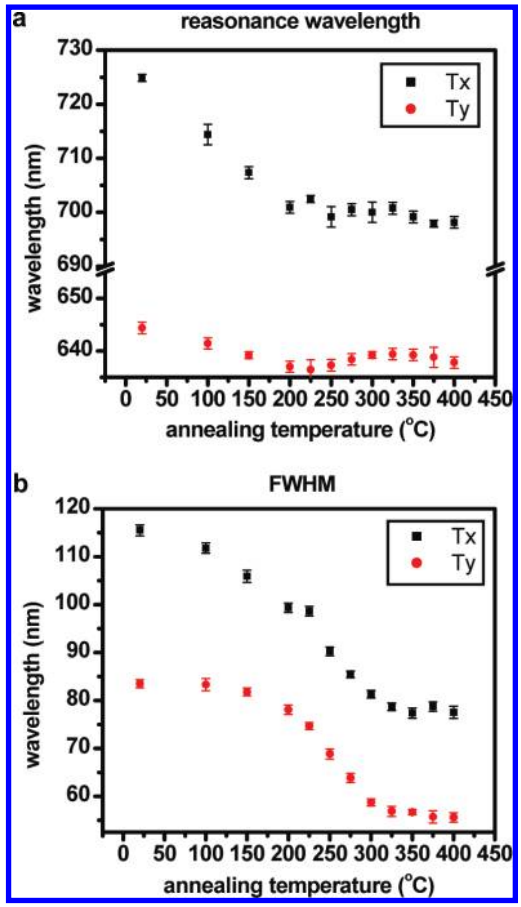

FIGURE 3. (a) Resonance wavelength and (b) resonance fwhm changes versus annealing temperature for both polarizations.

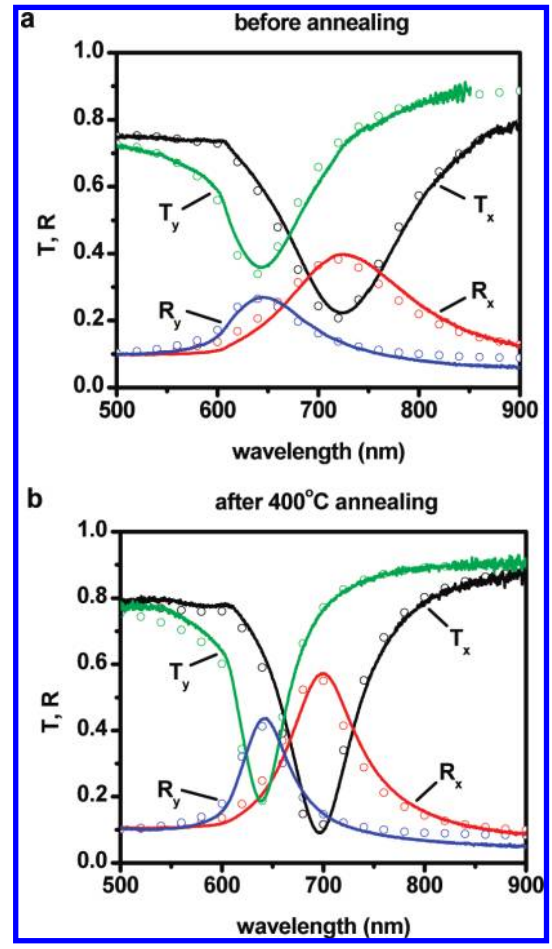

FIGURE 4. Experimental and simulated transmittance and reflectance spectra for (a) the original sample at room temperature and (b) the sample after 400 °C annealing. The black and green curves show the transmittance for x and y polarizations. Red and blue curves show the reflectance for x and y polarizations. The solid lines are experimental data, and the open circles are simulation data. The loss factor in the Drude model which is used for modeling is 3.54 in (a) and 1.35 in (b).

favorable orientations (plane parallel to the surface) will grow at the expense of grains with unfavorable orientations. A few grains grow very large by consuming other "unfavorable" grains. Improvement in the internal grain structure leads to a sharper resonance as quantified by a decreased fwhm.

More specifically, the improved grain structure results in a decreased $\varepsilon'' = \mathrm{Im}\,(\varepsilon)$, obtained from eq 1. Figure 4 shows a comparison between experimental spectra and numerical simulations obtained by finite element method (FEM) techniques. In fitting simulations to experiments, we use eq 1 with Drude parameters from Johnson and Christy (J&C) data[7] $\omega_p = 9$ eV and $\Gamma_p = 0.07$ eV, and with two Lorentzian oscillators with parameters as follows: $f_1 = 0.3$, $\omega_1 = 2.7$ eV, $\Gamma_1 = 0.3$ eV, $f_2 = 0.8$, $\omega_2 = 3.05$ eV, $\Gamma_2 = 0.5$ eV. The loss factor α is used to modify the gold damping term (Γ_p) to introduce the difference between J&C's bulk gold dielectric constant and the dielectric constant of the gold nanoantenna. The simulation parameters used to fit the experimental transmission and reflection data in Figure 4 show that the annealing treatment corresponds to a decrease in the loss factor of gold from 3.54 to 1.35 after annealing at 400 °C.

The shape and profile of the sample before and after 400 °C annealing are shown in panels a and b of Figure 5. From the images, it has been determined that there is only a small change (~3%) in the particle's dimension before and after annealing. From simulations, we know slight changes in the geometric dimensions are not equivalent to a change in loss factor, which represents the net effect of both the surface and internal structural quality of the metal. We also examine changes in surface quality using tilted FE-SEM and AFM measurements, shown in panels c and d of Figure 5 with a tilt angle of 60°. From the SEM, it can be seen that the surface roughness of the nanoantenna is smoother after annealing. Panels e and f of Figure 5 show AFM 3D images. In Figure 5e, small bumps signify the formation of small polycrystalline grains. Annealing creates larger grains, leading to smaller average roughness. The polycrystal grain structure could be the primary reason for surface roughness. In order to measure the surface roughness on the slightly curved surfaces of the square particle, a small area plane-fit (60 nm × 60 nm) is used before measuring roughness. The

DOI: 10.1021/nl9037246 | Nano Lett. 2010, 10, 916–922

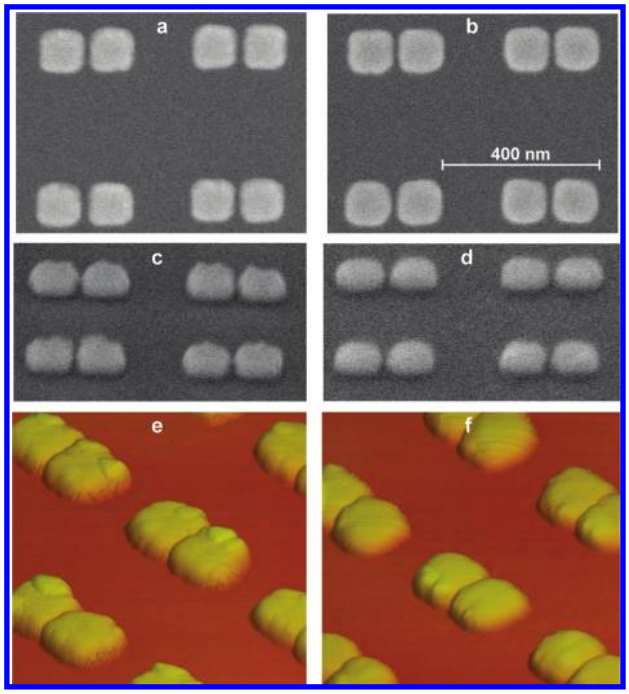

FIGURE 5. (a) SEM plane view image before annealing and (b) after annealing (the scale bar is 400 nm). (c) Tilted SEM (incident angle = 60°) before annealing and (d) after annealing. (e) AFM 3D image of the sample before and (f) after annealing (the image size is 1 μm × 1 μm).

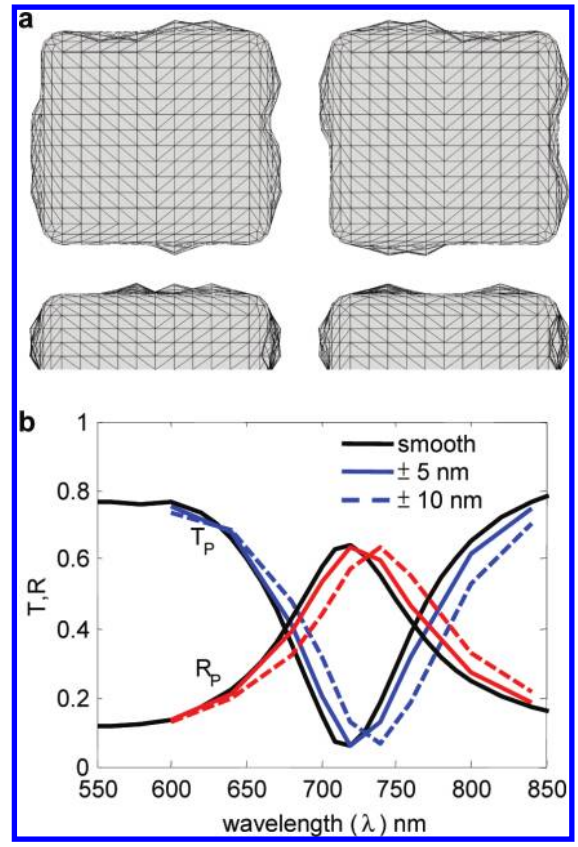

FIGURE 6. (a) An example FEM mesh of a nanoantenna pair with roughness (top and side view). (b) The resulting transmission and reflection spectra for the primary polarization for smooth, ±5 nm, and ±10 nm bump amplitudes.

rms roughness on the top of the nanoantenna is reduced from 2.57 to 1.73 nm after 400 °C annealing.

As has been discussed, surface roughness may contribute to loss factor, resulting in decreased resonance strength and broadening. However our simulations show that for moderate roughness, no significant changes are observed in the relaxation rate. To examine this effect, three-dimensional simulations of square-particle nanoantennas with surface roughness are shown in Figure 6. These simulations place displacement "bumps" over the surfaces of the nanoantennas, simulating roughness. Bump amplitudes of 0 nm (smooth), ±5 nm, and ±10 nm have shown that increased surface roughness may shift the resonance wavelength but does not significantly influence the loss factor. Note that roughness in the gaps may provide a significant contribution to the inhomogeneous broadening of a plasmon resonance. The effect of the gap size diversity was analyzed using representative nanoantennas similar those presented in panels a and b of Figure 5. One can see from Figure 5 and also more detail consideration shows that the roughness in the gap is less than 5 nm (R_{rms} measurements from panels a and b of Figure 5 in the gap are 2.5 nm before annealing and 2.4 nm after annealing) which means that the broadening is actually less than that simulated in Figure 6b with the solid blue line and can be estimated as about 2 nm, which is indeed not a significant contribution to the broadening. Therefore, we may conclude that significant changes in modeling loss factor after annealing are not due to surface improvement but are primarily due to changes in internal defects.

The internal metal grain structure was analyzed by using X-ray diffraction (XRD) measurement, where the crystal size is quantified by analyzing peak broadening of the Bragg reflections in the Cu Kα X-ray diffraction scans as taken in the $\theta/2\theta$ mode. The grain size (d_g) is determined from the (111) reflections using the standard Debye−Scherrer formulation.[23]

$$\text{average crystallite size } (d_g) = \frac{K\lambda}{B_{struc}\cos\theta} \qquad (2)$$

In eq 2 K describes the crystallite shape factor, λ is X-ray wavelength, and θ describes the angle of incidence. For our measurements K is taken to be 0.9, which is typical for spherical grains (K is in a range from 0.8 to 1 for possible variations in shape), λ is 0.514 nm for the copper anode. B_{struc}describes the structural broadening, which is the difference in the integral profile width as defined in eq 3

DOI: 10.1021/nl9037246 | *Nano Lett.* **2010,** *10,* 916–922

$$B_{\mathrm{struc}} = \sqrt{{B_{\mathrm{obs}}}^2 - {B_{\mathrm{std}}}^2} \quad (3)$$

where B_{obs} is the full-width measured at half-maximum intensity of the sample and B_{std} equals 0.19° as measured for an Au(111) single-crystal standard.[24]

Figure 7 shows the XRD $\theta/2\theta$ measurement of the nanoantenna sample before and after annealing. The Au(111) diffraction angles for both samples are 38.2° for the $\theta/2\theta$ measurement. B_{obs} of the original nanoantenna sample is 0.416° and B_{obs} of the annealed nanoantenna sample is 0.283°. Using eq 2, we may calculate that the average grain size has increased from 22 to 40 nm.

Note that the Debye−Scherrer formula implies just one, "average" size of the grains for any grain shape. This means that if the formula gives a grain size of 40 nm, larger than the thickness (31 nm after annealing), one can expect a slightly larger than 40 nm size in the $x-y$ plane.

In order to analyze the electron relaxation rate we use a quantitative model based on the linearized Boltzmann equation.[11] In this model, grain boundaries are represented as N parallel partially reflecting planes, located perpendicular to the electric field E, and placed an average random distance d apart. Mathematically, these planes are identified with scattering potentials of height U (energy) and width w (actually delta functions of strength $S = Uw$); inside the grains, the electron scattering is described by a relaxation time τ. If d is identified with the average grain diameter D, the model gives total relaxation time in the metal with grains, τ_g

$$\frac{\tau_g}{\tau} = 1 - 1.5\beta + 3\beta^2 - 3\beta^3 \ln(1 + \beta^{-1}) \quad (4)$$

where

$$\beta = \frac{v_F \tau}{D} \frac{R}{1 - R}$$

with the electron reflection coefficient, R, introduced from the potential barrier strength as $R/(1 - R) = S^2/\hbar^2$, and $v_F = 1.35 \times 10^6$ m/s is the Fermi velocity for Au.

The solution for inverse of the relaxation time (${\tau_g}^{-1} = \Gamma_g$) can be approximated by simple linear dependence on the inverse grain size D^{-1}

$${\tau_g}^{-1} = {\tau_0}^{-1} + \frac{1.37 v_F R}{D(1 - R)} \quad (5)$$

In this equation τ_0 is the relaxation time of infinite grain size. A choice of the reference relaxation rate for an infinite grain size requires special discussion. Careful consideration of possible sources show that there are not so many measurements where the contribution of grain size was determined. Data obtained by Motulevich for gold films is supported by grain contribution and grain size measurements.[12] Reference relaxation rate was determined from $\rho_{\mathrm{res}}/\rho = \nu_{\mathrm{ed}}/(\nu_{\mathrm{ep}} + \nu_{\mathrm{ed}})$, where the residual resistance ρ_{res} was measured at 4.2 K. The data by Motulevich show that the electron relaxation rate for infinite grain size is caused by electron−phonon collision rate ${\tau_0}^{-1} = \Gamma_0 = \Gamma_{\mathrm{ep}} = 26$ meV and grain contribution $\Gamma_{\mathrm{ed}} = 4$ meV with grain size about 200 nm.

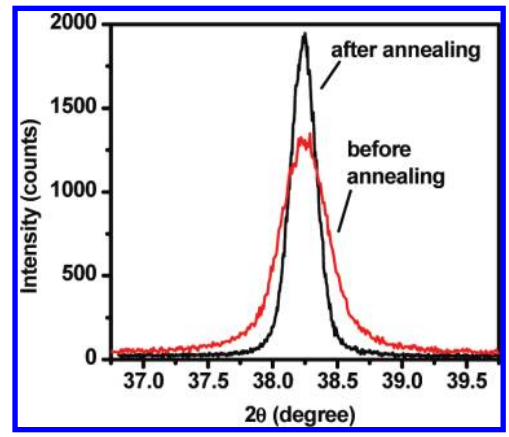

FIGURE 7. XRD $\theta/2\theta$ measurement of the nanoantenna before (black) and after (red) annealing.

TABLE 2. Comparison of the Electron Collision Rate and Grain Size for Nanoantennas, J&C,[7] and Motulevich's Data[12]

	before annealing	after annealing	J&C	Motulevich
Γ_g, meV	241	93	72	30
D, nm	22	40	50	200
R	0.78	0.67	0.64	0.39

The grain boundary reflection coefficient, R is often taken to be 0.5 as a first approximation.[25] One can see however from our data (Table 2) that the reflection coefficient can be different for nanoantennas before and after annealing likely due to a different volume fraction for the grain boundaries and, consequently, the strength of the scattering potentials. We should note that the difference in reflection coefficients between 0.7 and 0.8 makes a large difference in the relaxation rate for the same grain size, which is about 100 meV at 22 nm and much larger than the experimental error in the relaxation rate measurements.

To summarize, annealing not only increases the metal grain size but also reduces the reflection coefficient of the potential barriers. Both factors result in a substantially improved electron relaxation rate for nanostructures, leading to a value comparable with large area samples. The grain contribution to the electron relaxation rate is reduced by a factor of 3.2 due to the grain size being increased from 22 to 40 nm. Additionally the reflection coefficient has been reduced from 0.78 to 0.67.

Note that loss due to internal grains also explains our previous results for size-dependent permittivity with a large A-factor (the coefficient in the size dependence) and the

DOI: 10.1021/nl9037246 | Nano Lett. 2010, 10, 916–922

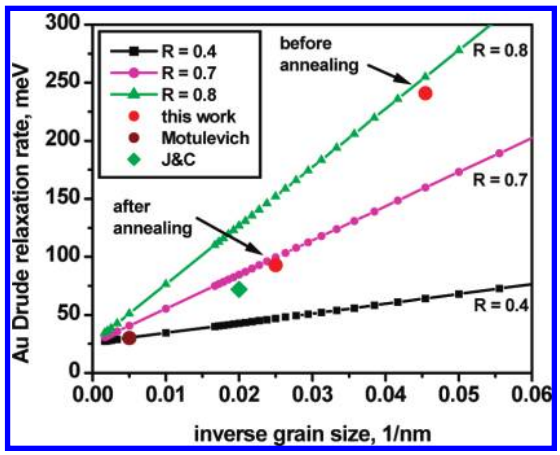

FIGURE 8. Au electron scattering rate, Γ_g ($\Gamma_0 = 26$ meV) calculated with the above model at $R = 0.4$, 0.7, and 0.8. The results for gold nanoantennas were plotted with red circles. The Motulevich result for gold is shown with a brown circle, while the Johnson and Christy result is depicted with a green diamond. The grain size is taken approximately equal to film thickness, 50 nm in the J&C[7] case.

observed independence on the surface roughness.[14] Indeed the large A-factor indicates that the grain size is more crucial than structure size. Also, the electron scattering at the grain boundaries would significantly affect the electron relaxation rate, more than that by surface roughness of the entire particle. The restructuring increases grain size and decreases the internal boundary reflection coefficient, both of which substantially improve the quality of the plasmon resonance.

Finally we qualitatively discuss whether the above results may be applied to nanostructures of different shape, size, and material (silver). Although annealing is shown to greatly improve the quality of gold nanoantennas by decreasing the electron relaxation rate, and similar results have been obtained for silver nanoantennas, some types of structures may not benefit from annealing, as discussed in the introduction. Heating initiates the Rayleigh instability and brakes strips into isolated particles. As with any instability the result depends on the initial conditions and driving forces; in the case of the strips, it depends on the width and initial quality of the gold. We also found that the absolute value of the dimensions is more important than aspect ratio; for example annealing does not improve quality in the case of 50 × 100 × 30 nm but does work for 100 × 200 × 30 nm. The gap dependence was studied for gold nanoantennas of a square shape. The positive results are almost independent of the gap size. Moreover if one takes slightly touching particles, they will separate during annealing at 400 °C, and it is possible to obtain nanoantennas with a very narrow gap.

Annealing can be applied to silver nanoantennas, but at lower temperatures, about 250 °C (lower temperature is expected; all the restructurings happen at the temperature which is a fraction of melting temperature; the melting point for silver is about 103 °C lower than that for gold, 961 °C versus 1064 °C). Significant narrowing of the plasmon resonance has been observed for silver nanoantennas as well.

Indeed the result of annealing shows a complex dependence on particle size, aspect ratio, and material. Therefore, optimal annealing conditions for specific sample types must be tailored to the individual parameters of the sample.

Acknowledgment. This work was supported in part by U.S. Army Research Office under Grants 50372-CH-MUR and 50342-PH-MUR.

REFERENCES AND NOTES

(1) Su, K. H.; Wei, Q. H.; Zhang, X.; Mock, J. J.; Smith, D. R.; Schultz, S. *Nano Lett.* **2003**, *3*, 1087–1090.
(2) Sundaramurthy, A.; Schuck, P. J.; Conley, N. R.; Fromm, D. P.; Kino, G. S.; Moerner, W. E. *Nano Lett.* **2006**, *6*, 355–360.
(3) Kim, S.; Jin, J. H.; Kim, Y. J.; Park, I. Y.; Kim, Y.; Kim, S. W. *Nature* **2008**, *453*, 757–760.
(4) Bakker, R. M.; Yuan, H. K.; Liu, Z. T.; Drachev, V. P.; Kildishev, A. V.; Shalaev, V. M.; Pedersen, R. H.; Gresillon, S.; Boltasseva, A. *Appl. Phys. Lett.* **2008**, *92*, No. 043101.
(5) Bakker, R. M.; Drachev, V. P.; Liu, Z. T.; Yuan, H. K.; Pedersen, R. H.; Boltasseva, A.; Chen, J. J.; Irudayaraj, J.; Kildishev, A. V.; Shalaev, V. M. *New J. Phys.* **2008**, *10*, 125022.
(6) Gupta, R.; Dyer, M. J.; Weimer, W. A. *J. Appl. Phys.* **2002**, *92*, 5264–5271.
(7) Johnson, P. B.; Christy, R. W. *Phys. Rev. B* **1972**, *6*, 4370–4379.
(8) Homola, J.; Yee, S. S.; Gauglitz, G. *Sens. Actuators, B* **1999**, *54*, 3–15.
(9) Huang, W. Y.; Qian, W.; El-Sayed, M. A.; Ding, Y.; Wang, Z. L. *J. Phys. Chem. C* **2007**, *111*, 10751–10757.
(10) Kuttge, M.; Vesseur, E. J. R.; Verhoeven, J.; Lezec, H. J.; Atwater, H. A.; Polman, A. *Appl. Phys. Lett.* **2008**, *93*, 113110.
(11) Mayadas, A. F.; Shatzkes, M.; Janak, J. F. *Appl. Phys. Lett.* **1969**, *14*, 345–347.
(12) Motulevich, G. P. *Optical properties of metals*; Skobel'tsyn, D. V., Ed.; Consultants Bureau: New York, 1973.
(13) Weber, M. J. *Handbook of optical materials*; CRC Press: Boca Raton, FL, 2003.
(14) Drachev, V. P.; Chettiar, U. K.; Kildishev, A. V.; Yuan, H. K.; Cai, W. S.; Shalaev, V. M. *Opt. Express* **2008**, *16*, 1186–1195.
(15) Kaiser, N. *Appl. Opt.* **2002**, *41*, 3053–3060.
(16) Kreibig, U. *J. Phys. F: Met. Phys.* **1974**, *4*, 999–1014.
(17) Hulteen, J. C.; Patrissi, C. J.; Miner, D. L.; Crosthwait, E. R.; Oberhauser, E. B.; Martin, C. R. *J. Phys. Chem. B* **1997**, *101*, 7727–7731.
(18) Habenicht, A.; Olapinski, M.; Burmeister, F.; Leiderer, P.; Boneberg, J. *Science* **2005**, *309*, 2043–2045.
(19) Huang, W.; El-Sayed, M. A. *Eur. Phys. J.-Spec. Topics* **2008**, *153*, 223–230.
(20) Zheng, Y. B.; Huang, T. J.; Desai, A. Y.; Wang, S. J.; Tan, L. K.; Gao, H.; Huan, A. C. H. *Appl. Phys. Lett.* **2007**, *90*, 183117.
(21) Yoshida, N.; Oshima, R.; Fujita, F. E. *J. Phys. F: Met. Phys.* **1972**, *2*, 237–246.
(22) Feltham, P. *Acta Metall.* **1957**, *5*, 97–105.
(23) Chen, G.; Hui, P.; Pita, K.; Hing, P.; Kong, L. *Appl. Phys. A: Mater. Sci. Process.* **2005**, *80*, 659–665.
(24) Jankowski, A. F.; Saw, C. K.; Harper, J. F.; Vallier, B. F.; Ferreira, J. L.; Hayes, J. P. *Thin Solid Films* **2006**, *494*, 268–273.
(25) Marsillac, S.; Barreau, N.; Khatri, H.; Li, J.; Sainju, D.; Parikh, A.; Podraza, N. J.; Collins, R. W. *Phys. Status Solidi C* **2008**, *5*, 1244–1248.

DOI: 10.1021/nl9037246 | *Nano Lett.* **2010,** *10,* 916–922